Revue des Composites et des Matériaux Avancés-Journal of Composite and Advanced Materials
Vol. 36, No. 5, October, 2026, pp. 1137-1144
Journal homepage: http://iieta.org/journals/rcma

Date Palm Seed Ash as a Sustainable Additive for Metakaolin-Based Geopolymers: Mechanical Performance and Pb^{2+} Adsorption

Faten Al-Slaty[1*], Tariq Bashiti[1], Madlin Amjad[1], Enas N. Mahmoud[2]

[1] Department of Earth and Environmental Sciences, Prince El Hassan bin Talal Faculty of Natural Resources and Environment, The Hashemite University, Zarqa 13133, Jordan
[2] Department of Chemistry, Faculty of Science, The Hashemite University, Zarqa 13133, Jordan

Corresponding Author Email: fatenm@hu.edu.jo

Copyright: ©2026 The authors. This article is published by IIETA and is licensed under the CC BY 4.0 license (http://creativecommons.org/licenses/by/4.0/).

https://doi.org/10.18280/rcma.360519

Received: 5 July 2026
Revised: 2 September 2026
Accepted: 15 September 2026
Available online: 31 October 2026

Keywords:
date palm seed ash, geopolymer, agricultural waste valorization, lead adsorption, heavy metal removal

ABSTRACT

This study investigates the use of date palm seed ash (DPSA) as a sustainable additive in the synthesis of metakaolin (MK)-based geopolymers. Geopolymers were prepared by partially replacing MK with DPSA at levels ranging from 10 to 50 wt.% and were characterized through chemical, mechanical, mineralogical, microstructural, and adsorption analyses. Among the investigated DPSA-containing mixtures, 30 wt.% DPSA was identified as the optimum replacement level, providing the best overall balance between mechanical and adsorption performance. The geopolymer containing 30 wt.% DPSA achieved a compressive strength of 28.42 MPa, a Brunauer–Emmett–Teller (BET) specific surface area (SSA) of 13.8 m^2 g^{-1}, a Pb^{2+} removal efficiency of 98%, and an adsorption capacity of 4.90 mg g^{-1}. X-ray diffraction (XRD) and scanning electron microscopy (SEM)–energy-dispersive X-ray spectroscopy (EDS) analyses confirmed the formation of a predominantly amorphous aluminosilicate geopolymer matrix containing secondary crystalline aluminosilicate phases. These findings demonstrate the potential of DPSA as a sustainable additive for producing MK-based geopolymers with satisfactory mechanical performance and enhanced Pb^{2+} adsorption.

1. INTRODUCTION

Geopolymers are alkali-activated aluminosilicate materials synthesized from silica- and alumina-rich precursors. Owing to their relatively low energy demand, reduced CO_2 emissions, and ability to valorize industrial and agricultural wastes, they have emerged as promising alternatives to ordinary Portland cement [1, 2]. Their three-dimensional aluminosilicate framework can provide favorable mechanical properties, chemical stability, and durability, making them suitable for a range of structural and environmental applications.

Biomass ashes have attracted increasing interest as geopolymer precursors because they enable the beneficial utilization of agricultural residues while reducing waste disposal impacts. The performance of biomass ash-based geopolymers is strongly influenced by the contents of reactive SiO_2, Al_2O_3, and CaO, which affect geopolymerization and the engineering properties of the resulting materials [2, 3]. Rice husk ash (RHA), one of the most extensively studied biomass ashes, has been shown to enhance geopolymerization, mechanical properties, durability, and environmental performance owing to its high amorphous silica content [4-7]. Similar benefits have been reported for sugarcane bagasse ash, coconut shell ash, corn cob ash, and palm oil fuel ash, indicating that the successful incorporation of biomass ashes is strongly influenced by their chemical composition, amorphous phase content, and replacement level [8-10].

Among the various agricultural residues investigated for geopolymer production, date palm (*Phoenix dactylifera*) biomass has attracted increasing attention because of its abundance in arid and semi-arid regions, particularly across the Middle East and North Africa. Date palm seeds, which account for approximately 10–15 wt.% of the fruit, are a major by-product of the date-processing industry and are generated in substantial quantities. However, they remain largely underutilized, making their valorization an important strategy for waste management and circular economy practices [11, 12]. More recently, the thermal conversion of date palm seeds into date palm seed ash (DPSA) has created new opportunities for its use as a sustainable additive in cementitious and alkali-activated systems [12-16]. Previous studies have demonstrated the potential of date palm-derived materials for environmental and construction purposes, including heavy-metal and dye adsorption, asphalt modification, lightweight brick production, cementitious composites, and geopolymer reinforcement using date palm fibres [17-24].

Beyond their structural applications, geopolymers have attracted considerable attention as adsorbents for wastewater treatment because of their interconnected porous structure, abundant active sites, and ion-exchange capacity, which facilitate the removal of toxic heavy metals from aqueous solutions [25]. Heavy metal contamination remains a major

environmental challenge owing to the persistence, toxicity, and bioaccumulative nature of these pollutants [26]. Lead Pb^{2+}, in particular, is of significant concern because of its widespread occurrence in industrial effluents and its adverse effects on human health. Among the available treatment technologies, adsorption is considered an effective and economical approach because of its simplicity, high removal efficiency, and relatively low energy demand. In this context, geopolymers have emerged as promising alternatives to conventional adsorbents owing to their chemically stable aluminosilicate framework and tunable pore structure. Furthermore, the incorporation of agricultural waste-derived materials may enhance adsorption performance while supporting waste valorization within a circular economy framework [2, 12, 15].

Despite the growing interest in biomass ash-based geopolymers, previous research has focused predominantly on conventional agricultural ashes, such as RHA, sugarcane bagasse ash, and palm oil fuel ash. In contrast, the incorporation of DPSA into metakaolin (MK)-based geopolymer systems remains insufficiently investigated, particularly with respect to its effects on geopolymerization, microstructural characteristics, mechanical performance, and heavy metal adsorption. To address this knowledge gap, the present study investigates the feasibility of using DPSA as a sustainable additive in MK-based geopolymers. The effects of DPSA incorporation on the physical, mechanical, mineralogical, microstructural, and Pb^{2+} adsorption properties of the synthesized geopolymers were systematically evaluated. By integrating agricultural waste valorization with environmental remediation, this study contributes to the development of geopolymer materials that combine satisfactory mechanical performance with enhanced initial Pb^{2+} adsorption capability.

2. MATERIALS AND METHODS

2.1 Materials and characterization

The Kaolin ore was collected from the Ma'an region in southern Jordan. The raw kaolin was crushed using a laboratory jaw crusher and sieved using a mechanical sieve shaker to obtain the fraction passing through an ASTM No. 200 sieve (<75 μm). The <75 μm fraction was calcined in a muffle furnace at 750 ℃ for 2 h to produce MK. After calcination, the material was allowed to cool naturally to room temperature and subsequently stored in sealed containers to minimize moisture uptake prior to geopolymer preparation.

Date palm seeds were collected from local date-processing factories in Jordan. The seeds were thoroughly washed with tap water to remove adhering impurities and oven-dried at 150 ℃. A total of 5 kg of dried seeds was combusted under open-air conditions in five separate batches of approximately 1 kg each. Each batch was burned for 30–45 min until complete ash formation was achieved, while the temperature was monitored and maintained at approximately 500–550 ℃. After cooling naturally to room temperature, the ash from all five batches was combined and thoroughly mixed to obtain a representative, homogeneous bulk sample and minimize batch-to-batch variability. The homogenized ash was subsequently sieved through an ASTM No. 200 sieve (<75 μm), and the fraction passing through the sieve was used for geopolymer preparation and characterization.

The chemical compositions of MK and DPSA were determined by X-ray fluorescence (XRF) using an S8 TIGER spectrometer (Bruker AXS, Germany). Their mineralogical compositions were characterized by X-ray diffraction (XRD) using an XRD-7000 diffractometer (Shimadzu, Japan) with Cu Kα radiation (λ = 1.5418 Å), operated at 40 kV and 30 mA. Phase identification was performed using the International Centre for Diffraction Data Powder Diffraction File-2 (ICDD PDF-2) database. The morphology and elemental composition of the raw materials and selected geopolymer specimens were examined by scanning electron microscopy (SEM) coupled with energy-dispersive X-ray spectroscopy (EDS); Quanta 600, FEI, USA, equipped with a Bruker EDS detector. The specific surface area (SSA) was determined by the Brunauer–Emmett–Teller (BET) method using nitrogen adsorption at 77 K. Prior to analysis, the samples were degassed under vacuum to remove physically adsorbed moisture and other volatile species. The SSA values were calculated from the adsorption isotherms over the appropriate relative-pressure range.

The Pb^{2+} adsorption performance was evaluated using batch adsorption experiments. Before testing, the materials were crushed and ground to a fine powder. For each experiment, 1.0 g of adsorbent was added to 50 mL of an aqueous solution containing 100 mg L^{-1} Pb^{2+}, prepared from $Pb(NO_3)_2$. The initial pH of the solution was 5.0. The suspensions were shaken at 150 rpm for 24 h at room temperature and subsequently filtered. The residual Pb^{2+} concentration in the filtrate was determined by atomic absorption spectroscopy (AAS; AAnalyst 400, PerkinElmer, USA). All experiments were performed in triplicate, and the reported values represent the mean of three independent measurements.

The Pb^{2+} removal efficiency (RE, %) and equilibrium adsorption capacity (q_e, mg g^{-1}) were calculated using Eqs. (1) and (2), respectively:

$$RE=(C_0-C_e)/C_0\times100\% \quad (1)$$

where, C_o and C_e (mg L^{-1}) are the initial and equilibrium Pb^{2+} concentrations, respectively.

$$q_e=[(C_0-C_e)\times V]/m \quad (2)$$

where, V (L) is the solution volume and m (g) is the mass of the adsorbent.

2.2 Geopolymer preparation and characterization

The alkaline activator consisted of a 10 M NaOH solution prepared from NaOH pellets (99% purity, Sigma-Aldrich, USA) and a commercial sodium silicate (Na_2SiO_3) solution containing 25.6–27.6 wt.% SiO_2 and 7.5–8.5 wt.% Na_2O. The activator was prepared by mixing the Na_2SiO_3 and NaOH solutions at a mass ratio of 1:1, followed by thorough stirring and equilibration at room temperature prior to use.

A series of geopolymer mixtures was prepared by partially replacing MK with DPSA at replacement levels of 10, 20, 30, 40, and 50 wt.% to determine the optimum replacement level. The NaOH concentration (10 M), Na_2SiO_3/NaOH mass ratio (1:1), and solid-to-liquid ratio (S/L = 2.0) were kept constant for all mixtures. The alkaline activator was gradually added to the dry precursors, and the mixtures were mechanically mixed for 2 min at 100 rpm, followed by 10 min at 200 rpm, until a homogeneous paste was obtained.

The fresh paste was cast into 50 × 50 × 50 mm steel moulds,

sealed with polyethylene film to minimize moisture loss, and cured at 100 °C for 24 h. After demoulding, the specimens were stored under ambient laboratory conditions for 7 days before testing. Three specimens were prepared and tested for each mixture, and the unconfined compressive strength (UCS) results are reported as the mean ± standard deviation (SD) of three independent measurements (n = 3).

The UCS of the synthesized geopolymers was measured using a universal testing machine (MATEST NS205N) at a loading rate of 5 mm min^{-1}. Selected geopolymer specimens were further characterized by XRD, SEM–EDS, BET SSA analysis, and Pb^{2+} adsorption experiments following the procedures described in Section 2.1.

3. RESULTS AND DISCUSSION

3.1 Chemical characterization

Table 1 presents the chemical compositions of MK and DPSA used in this study, together with DPSA compositions reported in previous studies (DPSA1 and DPSA2). The XRF results show that MK is predominantly aluminosilicate, with a combined SiO_2 and Al_2O_3 content of 91.6 wt.%, confirming its suitability as the primary precursor for geopolymer synthesis. The low contents of CaO, MgO, Na_2O, and K_2O, together with the low loss on ignition (LOI) (1.85 wt.%), indicate a silica- and alumina-rich composition that is generally favorable for alkaline activation.

In contrast, DPSA exhibited a markedly different oxide composition, with lower SiO_2 (19.5 wt.%) and Al_2O_3 (6.39 wt.%) contents but relatively high concentrations of K_2O (18.5 wt.%), P_2O_5 (18.2 wt.%), CaO (10.3 wt.%), and MgO (9.05 wt.%). This composition indicates that DPSA functions primarily as a mineral-rich sustainable additive rather than as the principal aluminosilicate precursor. The relatively high P_2O_5 content is consistent with previous studies showing that phosphorus in date palm seeds is predominantly stored as phytate, the principal phosphorus reserve required for seed germination and early seedling development [27]. During combustion, the organic fraction is largely removed, resulting in the enrichment of inorganic mineral constituents in the residual ash [11, 28]. Accordingly, the elevated concentrations of K_2O, CaO, MgO, and P_2O_5 observed in DPSA are consistent with the mineral composition of date seeds and their concentration in the ash following combustion.

Table 1. Chemical compositions of metakaolin (MK) and date palm seed ash (DPSA) used in the present study compared with DPSA compositions reported in previous studies

Material	SiO_2	Al_2O_3	Fe_2O_3	TiO_2	MnO	MgO	CaO	Na_2O	K_2O	P_2O_5	SO_3	Cl	LOI
MK	61.7	29.9	2.18	0.64	ND	0.52	0.33	0.32	0.89	ND	0.28	ND	1.85
DPSA	19.5	6.39	5.77	0.75	0.25	9.05	10.3	2.03	18.5	18.2	3.65	1.61	3.56
DPSA[1]	45.5	20.75	7.25	ND	0.32	0.52	9.82	3.00	9.07	0.50	0.12	0.45	1.72
DPSA[2]	0.89	ND	0.70	ND	ND	3.50	5.52	ND	43.02	7.40	2.77	5.54	4.8

Note: ND = Not determined. [1] [14]. [2] [19]. Loss on ignition (LOI).

Comparison with previously reported DPSA compositions reveals considerable variability in oxide contents. A silica-rich DPSA containing 45.5 wt.% SiO_2 and 20.75 wt.% Al_2O_3 was reported following controlled calcination at 630 °C for 8 h [14], whereas a substantially different composition was observed for DPSA produced by open-air combustion, with potassium as the dominant constituent and considerably lower silicon contents [19]. Such variability is expected because the chemical composition of biomass ash is strongly influenced by the date palm cultivar, geographical origin, soil characteristics, mineral uptake, combustion temperature and duration, and post-combustion ash processing [14, 28]. Furthermore, variations in thermal treatment conditions can alter the relative proportions of major oxides by affecting the removal of volatile constituents and the concentration of the remaining mineral phases.

The marked compositional differences between MK and DPSA indicate that the two materials play complementary rather than equivalent roles in the geopolymer system. While MK provides the reactive aluminosilicate species required for geopolymer gel formation, DPSA primarily contributes alkali and alkaline-earth elements together with phosphorus-rich mineral components. Consequently, the performance of the blended geopolymers is expected to depend on an appropriate balance between preserving sufficient geopolymer-forming constituents from MK and incorporating mineral components from DPSA.

3.2 Mechanical characterization

The effect of DPSA incorporation on the UCS of MK-based geopolymers is presented in Figure 1. The reference geopolymer prepared solely from MK-G exhibited the highest UCS of 30.33 MPa. The strength of the DPSA-containing mixtures varied with the replacement level. Among these mixtures, the geopolymer containing 30 wt.% DPSA exhibited the highest UCS (28.42 MPa), followed by those containing 10 wt.% (24.81 MPa) and 20 wt.% DPSA (18.64 MPa). Further increasing the DPSA content to 40 and 50 wt.% reduced the UCS to 14.67 and 10.78 MPa, respectively.

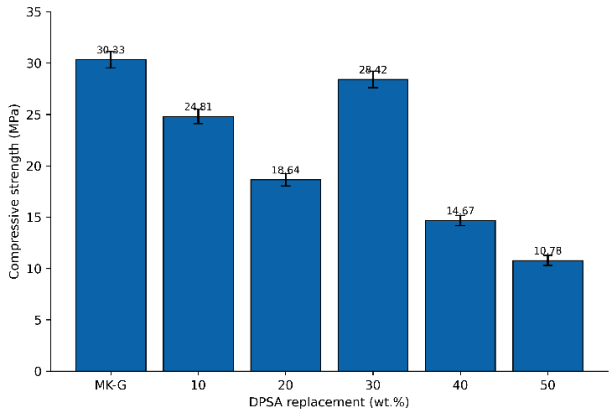


Figure 1. Compressive strength of MK-G and DPSA-containing geopolymers at different date palm seed ash (DPSA) replacement levels

Note: Values represent the mean of three specimens (n = 3), and error bars indicate ± standard deviation (SD).

Although none of the DPSA-containing mixtures exceeded

the strength of the reference geopolymer, the results indicate that 30 wt.% DPSA represents the optimum replacement level among the investigated compositions. At this level, the geopolymer maintained a compressive strength relatively close to that of the reference mixture, suggesting that moderate DPSA incorporation did not substantially compromise geopolymer matrix development. In contrast, higher DPSA contents resulted in a pronounced reduction in strength, which can be attributed to the progressive decrease in MK, the primary reactive aluminosilicate precursor. As demonstrated by the XRF results, DPSA contains considerably lower SiO_2 and Al_2O_3 contents than MK. Consequently, increasing the DPSA content reduces the availability of reactive Si- and Al-bearing species required for geopolymer gel formation. Moreover, the K-, Ca-, and P-bearing phases introduced by DPSA do not appear to compensate for the reduced availability of these reactive species at higher replacement levels, thereby limiting the development of a continuous geopolymer matrix.

A similar trend has been reported for other biomass ash-modified geopolymer systems. The incorporation of RHA into fly ash-based geopolymers was found to improve mechanical performance only within a limited replacement range, while excessive RHA contents reduced compressive strength because of dilution of the reactive precursor and the consequent decrease in geopolymer gel formation [4]. Similarly, the partial replacement of fly ash with biomass wood ash enhanced compressive strength up to an optimum level, beyond which the mechanical properties deteriorated [29]. Studies on DPSA used as a supplementary cementitious material have likewise shown that moderate replacement levels generally provide favorable mechanical performance, while excessive DPSA contents reduce strength because of dilution of the primary binder and the lower reactivity of the ash relative to the main cementitious precursor.

The present results therefore indicate that the mechanical performance of DPSA-containing geopolymers depends on maintaining sufficient MK to develop a continuous binding matrix, with 30 wt.% DPSA providing the best balance among the investigated replacement levels.

3.3 Mineralogical characterization

The XRD patterns of MK, DPSA, MK-G, and MK-30%DPSA-G are presented in Figure 2. The diffraction pattern of MK shows a marked reduction in the characteristic kaolinite reflection at approximately 12.4° (2θ), indicating that most of the kaolinite was transformed into MK during calcination. Nevertheless, weak residual kaolinite peaks remained detectable, suggesting incomplete transformation. Quartz remained the dominant crystalline phase, as evidenced by its prominent reflections at approximately 20.8°, 26.6°, and 36.5° (2θ), confirming its thermal stability under the applied calcination conditions. Minor reflections attributable to muscovite were also observed.

The XRD pattern of DPSA is dominated by a broad diffuse hump accompanied by only weak crystalline reflections, indicating that the ash consists predominantly of poorly crystalline or amorphous phases. Based on the XRF analysis, the amorphous fraction is likely associated with Si-, P-, K-, Ca-, and Mg-bearing constituents. However, XRD cannot distinguish individual amorphous components, and the absence of distinct crystalline phosphate reflections does not exclude the presence of phosphorus, which may occur in amorphous or poorly crystalline forms. These observations are consistent with previous studies showing that the mineralogical characteristics and reactivity of DPSA are strongly influenced by combustion conditions, particle fineness, and chemical composition, which affect the relative proportions of amorphous and crystalline phases in the resulting ash.

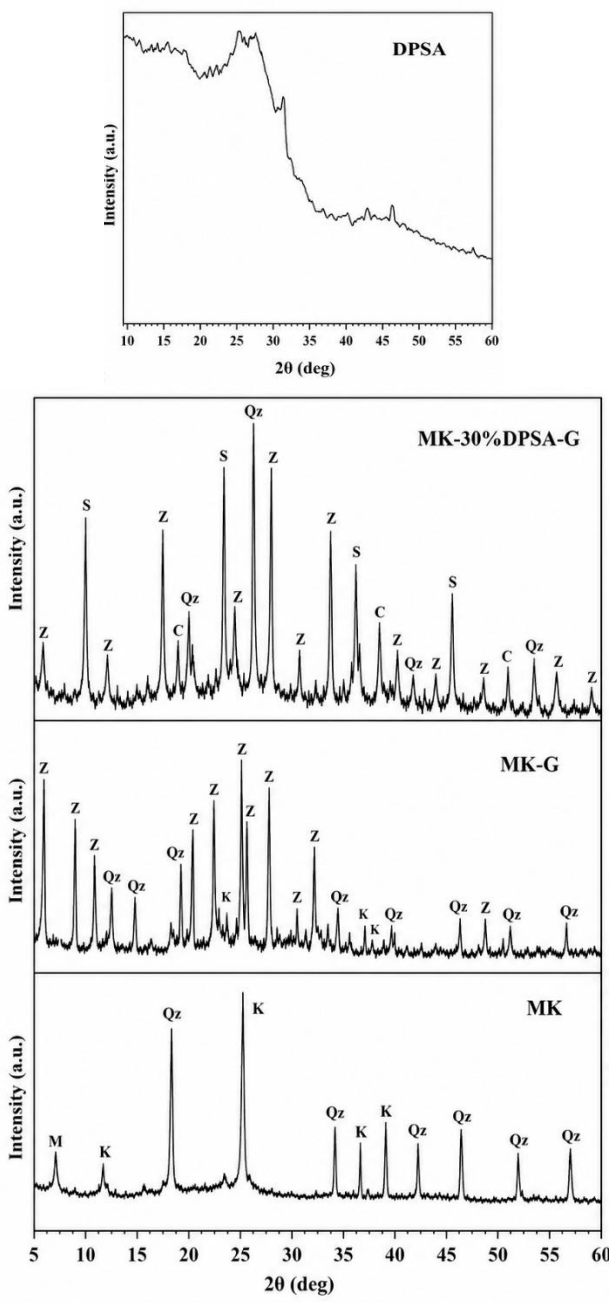


Figure 2. X-ray diffraction (XRD) patterns of metakaolin (MK), date palm seed ash (DPSA), MK-G, and MK-30%DPSA-G

Note: Peak labels indicate reflections assigned to Qz: quartz, M: muscovite, K: kaolinite, Z: zeolite phase, S: sodalite, and C: cancrinite.

Compared with MK, the XRD pattern of MK-G exhibited residual quartz together with several newly developed reflections, indicating the formation of crystalline reaction products during alkaline activation. Some reflections were tentatively assigned to zeolite-related phases, while minor residual kaolinite and muscovite remained detectable. These crystalline features were superimposed on a broad diffuse background, indicating that the reaction products consisted

mainly of an amorphous aluminosilicate geopolymer matrix containing secondary crystalline phases. Similar mineralogical characteristics have been reported for alkali-activated geopolymers, in which the binding matrix remains largely amorphous while limited crystalline aluminosilicate phases develop during curing. Furthermore, previous research has shown that precursor composition and activation conditions jointly influence the development of the geopolymer matrix and its associated physical properties, indicating that reaction-product formation depends on the overall mixture design rather than on a single constituent [30].

The incorporation of 30 wt.% DPSA resulted in further changes in the diffraction pattern. Residual quartz and zeolite-related reflections remained evident, while additional reflections tentatively assigned to sodalite and cancrinite were detected. The appearance of these crystalline aluminosilicate phases suggests that DPSA modified the chemical environment of the reacting system and influenced the crystallization pathway during geopolymerization. Although the study [12] focused on cementitious binders rather than geopolymers, it demonstrated the importance of interpreting mineralogical observations alongside complementary analyses, such as BET and microstructural characterization, when evaluating the performance of ash-containing binders. Accordingly, the XRD results in the present study are interpreted in conjunction with the SEM–EDS and BET observations rather than as independent evidence of material performance.

The persistence of a broad diffuse background in both geopolymer specimens indicates that the amorphous geopolymer gel remained the dominant binding phase despite the formation of secondary crystalline aluminosilicate phases. This mineralogical feature is consistent with the relatively high compressive strengths exhibited by MK-G and MK-30%DPSA-G; however, XRD alone cannot establish a direct relationship between phase composition and mechanical performance or quantify the relative proportions of amorphous and crystalline products. Therefore, the XRD observations should be interpreted in conjunction with the SEM microstructural analysis to better understand the geopolymer reaction products and their relationship to the measured mechanical properties.

3.4 Microstructural characterization

The SEM micrographs and corresponding EDS spectra of MK, DPSA, MK-G, and MK-30%DPSA-G are presented in Figure 3. The SEM image of MK (Figure 3(a)) shows irregular, angular particles with relatively smooth surfaces, characteristic of calcined kaolinitic materials. The particles exhibit a heterogeneous size distribution with no evidence of particle bonding or matrix formation. The corresponding EDS spectrum is dominated by oxygen (O), silicon (Si), and aluminum (Al), consistent with the aluminosilicate composition of MK. Minor amounts of potassium (K), magnesium (Mg), and iron (Fe) were also detected, consistent with the accessory mineral phases identified by XRD.

The DPSA micrograph (Figure 3(b)) exhibits a heterogeneous morphology consisting of fine particles together with a limited number of larger, irregular fragments. The corresponding EDS spectrum shows the presence of O, Si, Mg, P, K, Ca, and Fe, indicating a chemically diverse mineral composition. These observations are consistent with the XRF results, which revealed appreciable amounts of K-, P-, Ca-, and Mg-bearing constituents in DPSA. Furthermore, the detection of phosphorus by EDS, together with the absence of distinct crystalline phosphate reflections in the XRD pattern, suggests that at least part of the phosphorus may occur in amorphous or poorly crystalline forms. This interpretation is consistent with previous studies showing that the physicochemical characteristics of DPSA are strongly influenced by thermal processing and ash composition, which affect the relative proportions of crystalline and amorphous phases.

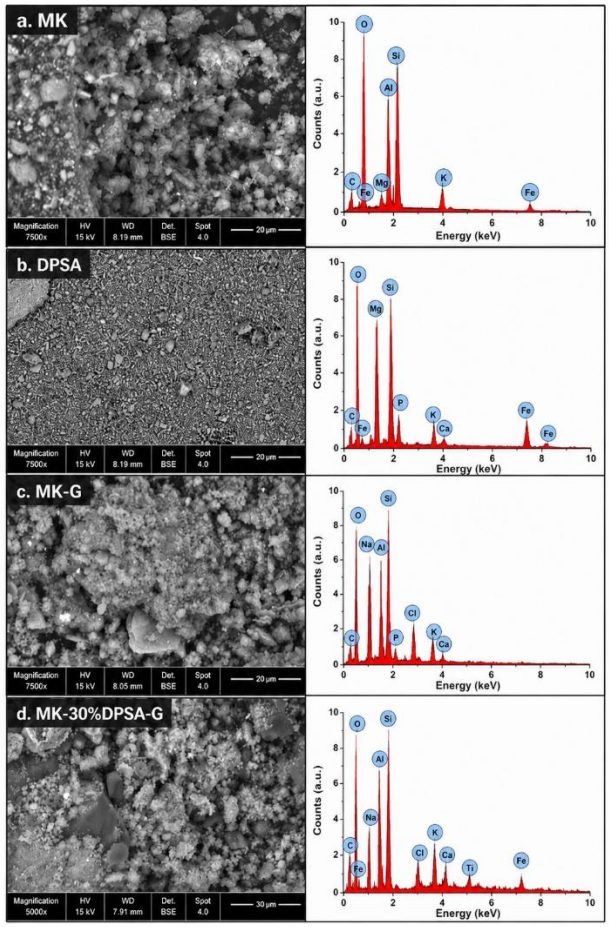


Figure 3. Microstructural images of (a) metakaolin (MK), (b) date palm seed ash (DPSA), (c) MK-G, and (d) MK-30%DPSA-G

Following alkaline activation, the morphology of MK-G (Figure 3(c)) changed markedly compared with that of the raw MK. The microstructure consists of agglomerated particles embedded within a relatively continuous reaction matrix, with some partially reacted particles remaining distinguishable. These features are characteristic of geopolymerized systems in which precursor dissolution and the formation of aluminosilicate reaction products occur during alkaline activation. The corresponding EDS spectrum is dominated by O, Si, Al, and Na, with minor amounts of P, Cl, K, and Ca also detected. The presence of Na is attributed to the sodium-based alkaline activator used in geopolymer synthesis. Similar microstructural characteristics have been reported for alkali-activated geopolymers, in which precursor composition and activation conditions influence matrix development and the persistence of partially reacted particles.

The incorporation of 30 wt.% DPSA further modified the morphology of the geopolymer (Figure 3(d)). The

microstructure appears more heterogeneous than that of MK-G, comprising agglomerated particles, irregular voids, and partially reacted grains. The corresponding EDS spectrum shows the presence of O, Si, Al, Na, K, Ca, Ti, and Fe. Compared with MK-G, the detection of K and Ca is consistent with the contribution of mineral constituents derived from DPSA to the geopolymer system. The coexistence of these elements with the dominant Si- and Al-bearing components indicates that DPSA modified the local chemical composition while maintaining the predominantly aluminosilicate character of the binding matrix. These microstructural and compositional observations should be interpreted in conjunction with the XRD and BET results when assessing the relationship between DPSA incorporation and geopolymer performance [12].

The SEM observations indicate that alkaline activation substantially modified the morphology of the raw materials, producing a more continuous reaction matrix while retaining some partially reacted particles. The SEM–EDS results are consistent with the XRF and XRD analyses, supporting the predominantly aluminosilicate character of the synthesized geopolymers and the contribution of mineral constituents derived from DPSA. Nevertheless, SEM–EDS provides primarily qualitative information; therefore, the microstructural observations should be interpreted in conjunction with the XRD, XRF, and mechanical characterization results to obtain a more comprehensive understanding of the geopolymer reaction products and their relationship to mechanical performance.

The XRD and SEM–EDS observations provide a microstructural basis for interpreting the UCS results. The high compressive strength of MK-G (30.33 MPa) is consistent with the predominantly amorphous aluminosilicate geopolymer matrix identified by XRD and the relatively continuous reaction matrix observed by SEM, suggesting effective bonding among the reacted precursor particles. Incorporation of 30 wt.% DPSA modified the reaction environment, as indicated by the appearance of secondary aluminosilicate phases tentatively assigned to sodalite and cancrinite and by the more heterogeneous microstructure containing irregular voids and partially reacted particles. Despite these features, sufficient MK remained available to maintain the continuity of the aluminosilicate binding matrix, enabling MK-30%DPSA-G to retain a relatively high UCS of 28.42 MPa. At higher DPSA replacement levels, the progressive decrease in MK reduces the availability of reactive Si- and Al-bearing species required for geopolymer gel formation, as supported by the substantially lower SiO_2 and Al_2O_3 contents of DPSA compared with MK. This dilution of the primary reactive precursor is expected to reduce gel continuity and increase structural heterogeneity, providing a plausible explanation for the decrease in UCS to 14.67 and 10.78 MPa at 40 and 50 wt.% DPSA, respectively. Thus, the mechanical performance reflects a balance between maintaining a sufficiently continuous aluminosilicate binding matrix and incorporating DPSA-derived constituents, with 30 wt.% representing the most favorable replacement level among the DPSA-containing mixtures.

3.5 Surface area and Pb^{2+} adsorption performance

The BET SSA and Pb^{2+} adsorption performance of the raw materials and selected geopolymer specimens are summarized in Figure 4. The results indicate that Pb^{2+} adsorption performance cannot be explained by SSA alone and is likely influenced by both the accessible surface characteristics and the chemical composition of the investigated materials.

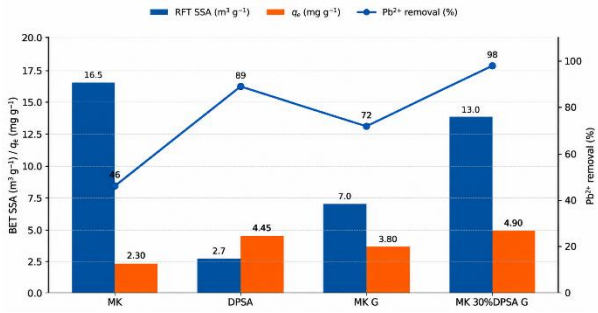


Figure 4. Brunauer–Emmett–Teller (BET) specific surface area (SSA) and Pb^{2+} adsorption performance of the raw materials and selected geopolymer specimens

Among the raw materials, MK exhibited the highest BET SSA (16.5 $m^2\ g^{-1}$), whereas DPSA showed a considerably lower value (2.7 $m^2\ g^{-1}$). Despite this difference, DPSA achieved a substantially higher Pb^{2+} removal efficiency (89%) and adsorption capacity (4.45 mg g^{-1}) than MK (46% and 2.30 mg g^{-1}, respectively). These results indicate that Pb^{2+} adsorption was not governed solely by accessible surface area, suggesting that the chemical and mineralogical characteristics of the adsorbents also influenced their adsorption performance. A similar relationship was reported in this study [31], where date seed ash effectively removed boron despite its relatively low BET SSA, further indicating that adsorption performance may depend on physicochemical characteristics in addition to surface area.

Following geopolymerization, the reference geopolymer (MK-G) exhibited a BET SSA of 7.0 $m^2\ g^{-1}$, a Pb^{2+} removal efficiency of 72%, and an adsorption capacity of 3.60 mg g^{-1}. Incorporation of 30 wt.% DPSA increased the BET SSA to 13.8 $m^2\ g^{-1}$ and resulted in the highest Pb^{2+} removal efficiency (98%) and adsorption capacity (4.90 mg g^{-1}) among the investigated specimens.

The approximately twofold increase in BET SSA relative to MK-G indicates that DPSA incorporation modified the accessible surface characteristics of the geopolymer matrix, potentially increasing the number of sites available for interaction with Pb^{2+}. This interpretation is also consistent with the more heterogeneous morphology and irregular voids observed by SEM for MK-30%DPSA-G. Previous studies have shown that the pore structure and accessible surface area of geopolymers can influence heavy-metal adsorption by affecting the availability of binding sites [32-34]. However, because pore-size distribution and total pore-volume data were not determined in the present study, the increase in BET SSA cannot be specifically attributed to the development of micropores or mesopores. Therefore, the present results indicate an increase in accessible SSA rather than direct evidence of changes in micro- or mesoporous structure. Moreover, surface area alone cannot explain the observed Pb^{2+} uptake, as MK exhibited a considerably higher BET SSA than DPSA (16.5 versus 2.7 $m^2\ g^{-1}$), while DPSA showed substantially greater Pb^{2+} removal (89% versus 46%). This contrast suggests that Pb^{2+} adsorption was influenced by both accessible surface characteristics and the chemical and mineralogical properties of the adsorbent. Accordingly, the enhanced adsorption performance of MK-30%DPSA-G is

interpreted as resulting from the combined influence of its increased accessible surface area and the modified chemical and mineralogical characteristics introduced by DPSA. Further pore-volume and pore-size distribution analyses would be required to determine the specific contribution of micro- and mesoporous structures.

It should be noted that the present study evaluates the initial Pb^{2+} adsorption capability of the synthesized geopolymers under the investigated batch conditions. The post-adsorption stability, Pb^{2+} leaching behaviour, and regeneration performance were not evaluated; therefore, further leaching and reuse studies are required before the practical applicability of these materials in wastewater treatment can be established.

4. CONCLUSIONS

This study demonstrated the feasibility of incorporating DPSA as a partial replacement for MK in alkali-activated geopolymers. XRD and SEM–EDS analyses indicated the formation of predominantly amorphous aluminosilicate geopolymer matrices containing secondary crystalline phases, while DPSA incorporation modified the mineralogical and microstructural characteristics of the synthesized geopolymers. Although the reference geopolymer (MK-G) exhibited the highest compressive strength (30.33 MPa), the incorporation of 30 wt.% DPSA provided the best overall balance between mechanical and adsorption performance, achieving a compressive strength of 28.42 MPa, the highest BET SSA among the geopolymer specimens (13.8 $m^2 g^{-1}$), and the highest Pb^{2+} removal efficiency (98%), with an adsorption capacity of 4.90 mg g^{-1}. These results indicate that Pb^{2+} adsorption was influenced not only by accessible SSA but also by the chemical, mineralogical, and microstructural characteristics of the adsorbent. Overall, the findings demonstrate the potential of DPSA as a sustainable additive for producing MK-based geopolymers with satisfactory mechanical performance and high initial Pb^{2+} adsorption capability. However, further investigations into long-term durability, post-adsorption Pb^{2+} leaching stability, adsorbent regeneration and reuse, optimization of mixture design and curing conditions, and performance under practical conditions are required before the suitability of DPSA-containing geopolymers for construction or wastewater treatment applications can be established.

ACKNOWLEDGMENT

The authors gratefully acknowledge the financial support provided by the Deanship of Scientific Research at The Hashemite University. The authors also thank the laboratory staff at the Royal Scientific Society (RSS), Jordan, for their technical assistance and analytical support.

REFERENCES

[1] Gökçe, H.S., Tuyan, M., Nehdi, M.L. (2021). Alkali-activated and geopolymer materials developed using innovative manufacturing techniques: A critical review. Construction and Building Materials, 303: 124483. https://doi.org/10.1016/j.conbuildmat.2021.124483

[2] Fernando, S., Gunasekara, C., Law, D.W., Nasvi, M.C.M., Setunge, S., Dissanayake, R. (2021). Life cycle assessment and cost analysis of fly ash–rice husk ash blended alkali-activated concrete. Journal of Environmental Management, 295: 113140. https://doi.org/10.1016/j.jenvman.2021.113140

[3] Ardhira, P.J., Shukla, S.K., Sathyan, D. (2024). Synthesis of geopolymer mortar from biomass ashes and forecasting its compressive strength behaviour. Case Studies in Construction Materials, 21: e03581. https://doi.org/10.1016/j.cscm.2024.e03581

[4] Detphan, S., Chindaprasirt, P. (2009). Preparation of fly ash and rice husk ash geopolymer. International Journal of Minerals, Metallurgy and Materials, 16(6): 720-726. https://doi.org/10.1016/S1674-4799(10)60019-2

[5] Hwang, C.L., Huynh, T.P. (2015). Effect of alkali-activator and rice husk ash content on strength development of fly ash and residual rice husk ash-based geopolymers. Construction and Building Materials, 101: 1-9. https://doi.org/10.1016/j.conbuildmat.2015.10.025

[6] Yomthong, K., Wattanasiriwech, S., Wattanasiriwech, D. (2019). Rice husk ash-geopolymer composite. IOP Conference Series: Materials Science and Engineering, 600(1): 012003. https://doi.org/10.1088/1757-899X/600/1/012003

[7] Liang, G., Liu, T., Li, H., Dong, B., Shi, T. (2022). A novel synthesis of lightweight and high-strength green geopolymer foamed material by rice husk ash and ground-granulated blast-furnace slag. Resources, Conservation and Recycling, 176: 105922. https://doi.org/10.1016/j.resconrec.2021.105922

[8] Olivia, M., Wulandari, C., Sitompul, I.R., Darmayanti, L., Djauhari, Z. (2016). Study of fly ash (FA) and palm oil fuel ash (POFA) geopolymer mortar resistance in acidic peat environment. In Materials Science Forum, Trans Tech Publications Ltd, 841: 126-132. https://doi.org/10.4028/www.scientific.net/MSF.841.126

[9] Yadav, A.L., Sairam, V., Srinivasan, K., Muruganandam, L. (2020). Synthesis and characterization of geopolymer from metakaolin and sugarcane bagasse ash. Construction and Building Materials, 258: 119231. https://doi.org/10.1016/j.conbuildmat.2020.119231

[10] Ngui, F., Mutai, V.K., Muhammed, N., Mutunga, F.M., Marangu, J.M., Otieno, M. (2024). Strength and durability performance of hybrid alkaline clay brick waste–coconut shell ash cement. Journal of Sustainable Construction Materials and Technologies, 9(4): 374-390. https://doi.org/10.47481/jscmt.1607846

[11] Al-Farsi, M.A., Lee, C.Y. (2008). Nutritional and functional properties of dates: A review. Critical Reviews in Food Science and Nutrition, 48(10): 877-887. https://doi.org/10.1080/10408390701724264

[12] Nasir, M., Al-Kutti, W. (2018). Performance of date palm ash as a cementitious material by evaluating strength, durability, and characterization. Buildings, 9(1): 6. https://doi.org/10.3390/buildings9010006

[13] Al-Kutti, W., Saiful Islam, A.B.M., Nasir, M. (2019). Potential use of date palm ash in cement-based materials. Journal of King Saud University–Engineering Sciences, 31(1): 26-31. https://doi.org/10.1016/j.jksues.2017.01.004

[14] Smith, A.S.J., Xu, G., Garba, M.J., Aliyu, M.Y. (2020). Pozzolanic and mechanical properties of date palm seed

ash (DPSA) concrete. Nigerian Journal of Technology, 39(3): 680-686. https://doi.org/10.4314/njt.v39i3.5

[15] Auta, I.B., Abdulkarim, I.I., Olu, O.O. (2023). Effect of date palm seed pod ash and eggshell powder on the physico-mechanical properties of cement blends. American Journal of Science, Engineering and Technology, 8(1): 1-11. https://doi.org/10.11648/j.ajset.20230801.11

[16] Mourak, A., Hajjaji, M. (2024). Moroccan heated clay-based geopolymer reinforced with date palm cellulose: Microstructure characterization and mechanical/physical properties. Clay Minerals, 59(1): 50-62. https://doi.org/10.1180/clm.2024.6

[17] Banat, F., Al-Asheh, S., Al-Makhadmeh, L. (2003). Evaluation of the use of raw and activated date pits as potential adsorbents for dye containing waters. Process Biochemistry, 39(2): 193-202. https://doi.org/10.1016/S0032-9592(03)00065-7

[18] Al-Ghouti, M.A., Li, J., Salamh, Y., Al-Laqtah, N., Walker, G., Ahmad, M.N. (2010). Adsorption mechanisms of removing heavy metals and dyes from aqueous solution using date pits solid adsorbent. Journal of Hazardous Materials, 176(1-3): 510-520. https://doi.org/10.1016/j.jhazmat.2009.11.059

[19] Gunarani, G.I., Chakkravarthy, S.P. (2017). Experimental studies on effect of date seed ash (DSA) on strength properties of cement sand mortar. IOP Conference Series: Earth and Environmental Science, 80(1): 012015. https://doi.org/10.1088/1755-1315/80/1/012015

[20] Al-Ithari, A.J., Sathasivan, A., Ahmed, R., Vuthaluru, H.B., Zhan, W., Ahmed, M. (2011). Superiority of date seed ash as an adsorbent over other ashes and ferric chloride in removing boron from seawater. Desalination and Water Treatment, 32(1-3): 324-328. https://doi.org/10.5004/dwt.2011.2717

[21] AlKheder, S., Alkhedher, M., Alshraiedeh, K.A. (2021). The effect of using activated dates seed on hot mix asphalt performance. Construction and Building Materials, 269: 121239. https://doi.org/10.1016/j.conbuildmat.2020.121239

[22] Limami, H., Manssouri, I., Cherkaoui, K., Khaldoun, A. (2021). Physicochemical, mechanical and thermal performance of lightweight bricks with recycled date pits waste additives. Journal of Building Engineering, 34: 101867. https://doi.org/10.1016/j.jobe.2020.101867

[23] Alshaaer, M., Alqahtani, O., Alharbi, M.M., et al. (2022). Synthesis and characterization of date palm fiber-reinforced geopolymer composite. Arabian Journal for Science and Engineering, 47(10): 12323-12332. https://doi.org/10.1007/s13369-021-06378-w

[24] Chkala, H., Kirm, I., Ighir, S., Ourmiche, A., Chigr, M., El Mansouri, N.E. (2024). Preparation and characterization of eco-friendly composite based on geopolymer and reinforced with date palm fiber. Arabian Journal of Chemistry, 17(2): 105510. https://doi.org/10.1016/j.arabjc.2023.105510

[25] Kumar, H., Sahoo, P.K., Mittal, S. (2021). Sustainable remediation of heavy metals: A review of current status and its future prospects. In New Trends in Removal of Heavy Metals from Industrial Wastewater. Elsevier, pp. 571-610. https://doi.org/10.1016/B978-0-12-822965-1.00023-4

[26] Zaynab, M., Al-Yahyai, R., Ameen, A., et al. (2022). Health and environmental effects of heavy metals. Journal of King Saud University-Science, 34(1): 101653. https://doi.org/10.1016/j.jksus.2021.101653

[27] Raboy, V. (2003). Myo-Inositol-1, 2, 3, 4, 5, 6-hexakisphosphate. Phytochemistry, 64(6): 1033-1043. https://doi.org/10.1016/S0031-9422(03)00446-1

[28] Habib, H.M., Ibrahim, W.H. (2009). Nutritional quality evaluation of eighteen date pit varieties. International Journal of Food Sciences and Nutrition, 60(sup1): 99-111. https://doi.org/10.1080/09637480802314639

[29] Abdulkareem, O.A., Matthews, J.C., Bakri, A.M.M.A. (2018). Strength and porosity characterizations of blended biomass wood ash-fly ash-based geopolymer mortar. AIP Conference Proceedings, 2045(1): 020096. https://doi.org/10.1063/1.5080909

[30] Emdadi, Z., Asim, N., Amin, M.H., et al. (2017). Development of green geopolymer using agricultural and industrial waste materials with high water absorbency. Applied Sciences, 7(5): 514. https://doi.org/10.3390/app7050514

[31] Al. Haddabi, M., Ahmed, M., Al. Jebri, Z., Vuthaluru, H., Znad, H., Al. Kindi, M. (2016). Boron removal from seawater using date palm (Phoenix dactylifera) seed ash. Desalination and Water Treatment, 57(11): 5130-5137. https://doi.org/10.1080/19443994.2014.1000385

[32] Tan, T.H., Mo, K.H., Ling, T.C., Lai, S.H. (2020). Current development of geopolymer as alternative adsorbent for heavy metal removal. Environmental Technology & Innovation, 18: 100684. https://doi.org/10.1016/j.eti.2020.100684

[33] Chen, S., Ruan, S., Zeng, Q., et al. (2022). Pore structure of geopolymer materials and its correlations to engineering properties: A review. Construction and Building Materials, 328: 127064. https://doi.org/10.1016/j.conbuildmat.2022.127064

[34] Lu, M., Chen, Y., Chen, S., et al. (2023). Potentiality of the porous geopolymer sphere in adsorption of Pb (II) from aqueous solutions: Behaviors and mechanisms. Ceramics International, 49(1): 698-706. https://doi.org/10.1016/j.ceramint.2022.09.040